Tellus SERIES B CHEMICAL AND PHYSICAL METEOROLOGY
PUBLISHED BY THE INTERNATIONAL METEOROLOGICAL INSTITUTE IN STOCKHOLM

Tellus (2008), 60B, 537–550
Printed in Singapore. All rights reserved

TELLUS

Response of the terrestrial carbon cycle to the El Niño-Southern Oscillation

By HAIFENG QIAN[1], RENU JOSEPH[1] and NING ZENG[1,2]*, [1]*Department of Atmospheric and Oceanic Science, University of Maryland, College Park, MD, 20740, USA;* [2]*Earth System Science Interdisciplinary Center, University of Maryland, College Park, MD, 20740, USA*

(Manuscript received 26 October 2007; in final form 7 April 2008)

ABSTRACT

Land plays a dominant role in the interannual variability of the global carbon cycle. The canonical warming and drying of the terrestrial tropics observed during El Niño events calls for the study of the role of precipitation and temperature on carbon cycle variability. Here we use a dynamic vegetation and terrestrial carbon model vegetation-global-atmosphere-soil (VEGAS) to investigate the response of terrestrial carbon cycle to El Niño-Southern Oscillation (ENSO) for the period 1980–2004. The simulated global total land–atmosphere flux (F_{ta}) by VEGAS agrees well with the atmospheric CO_2 inversion modelling results on ENSO timescales and is dominated by the tropics. Analysis of composites of terrestrial responses and climate factors during ENSO events and lead–lag correlations have identified that in the tropics, anomalous precipitation lags ENSO by 1 month and temperature by 5–6 months, while simulated soil moisture lags by 5 months. Warmer and drier conditions there cause suppression of Net Primary Production (NPP) and enhancement of Heteotrophic Respiration (R_h) simultaneously, resulting in the lagging of tropical F_{ta} by 6 months. Sensitivity simulations reveal that 2/3 of F_{ta} change comes from NPP and 1/3 from R_h. In VEGAS, fire burning accounts for about 25% of total F_{ta} anomalies. Precipitation during ENSO events contributes 56% of variation of F_{ta}; temperature accounts for 44%, which includes 25% from the enhancement of R_h and 7% from the increase of the vegetation respiration. We identify the remaining 12% variation of F_{ta} to be from an indirect effect of temperature through its effect on soil wetness, which in turn affects NPP. Such insight into the direct and indirect effects of climatic factors highlights the critical role of soil moisture in ecosystem and carbon cycle–a poorly constrained factor.

1. Introduction

The concentration of CO_2 in the atmosphere contributes significantly to the rate of global warming. Since the beginning of the industrial era, it had risen from about 280 ppmv to nearly 384 ppmv in 2007, with a 0.6 K increase of global mean temperature in the past century. The records of atmospheric CO_2 at Mauna Loa since 1958 indicate that besides the seasonal cycle, substantial interannual variability of atmospheric CO_2 is superimposed on the ongoing elevated atmospheric CO_2 concentration. An association between CO_2 growth rate and El Niño-Southern Oscillation (ENSO; Fig. 1) was initially reported in the 1970s and has been confirmed by recent statistical analysis (Bacastow, 1976; Keeling and Revelle, 1985; Braswell et al., 1997; Rayner et al., 1999; Jones et al., 2001; Zeng et al., 2005a). It was noticed that during El Niño (La Niña) events, the atmospheric CO_2 growth rate increased (decreased) at Mauna Loa station with a 5 month lag.

Climate driven variations in the global carbon cycle have been attributed as the primary cause of the interannual variability of atmospheric CO_2 growth rate, after accounting for long-term trends of fossil fuel emission and land use change. Oceanic measurements and inverse modelling studies found that the interannual variability of oceanic fluxes of CO_2 is relatively modest (Keeling and Revelle, 1985; Bousquet et al., 2000; Feely et al., 2002; Rödenbeck et al., 2003). Such an oceanic carbon flux variation points to the dominant role of the terrestrial biosphere in contributing to the interannual variability of global carbon flux. Bousquet et al. (2000) found that the global terrestrial carbon flux was approximately twice as variable as ocean fluxes, based on an inverse modelling study with 20 yr of CO_2 measurements.

The climate response of ENSO over land lags the tropical sea surface temperature (SST) signal by several months, resulting in variations in regional temperature, precipitation and radiation for terrestrial biosphere (Rasmusson and Carpenter, 1982; Trenberth et al., 1998; Potter et al., 2003; Joseph and Nigam, 2006). The typical El Niño events are characterized by changes in

*Corresponding author.
e-mail: zeng@atmos.umd.edu
DOI: 10.1111/j.1600-0889.2008.00360.x

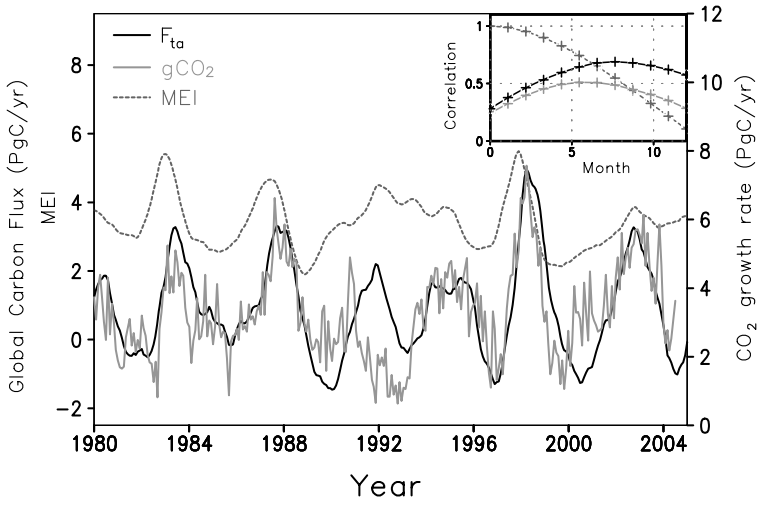

Fig. 1. Time-series indicating the correspondence of the CO_2 growth rate (gCO_2) at Mauna Loa, Hawaii and global total land–atmosphere carbon flux simulated by VEGAS and their lag with the MEI (units, dimensionless), which is shifted up by 3 units. The seasonal cycle has been removed with a filter of 12-month running mean. The right-hand top panel is the lagged correlation of MEI, F_{ta} and atmospheric CO_2 growth rate with MEI where the *x*-axis indicates the time lag in months. Value of 0.33 is statistically significant at the 90% level of Student's *t*-test.

atmospheric circulation and precipitation patterns (Ropelewski and Halpert, 1987) that give rise to warmer and drier conditions in the tropical land regions. Such a pervasive influence is likely to exert an impact on the land–atmosphere carbon exchange. Those physical and biological responses of terrestrial ecosystem to climate variation, especially to ENSO cycle, however, are not well known. Different climatic responses have been suggested in previous studies to be the primary cause of ENSO-related terrestrial carbon cycle variation. For example, Kindermann et al. (1996) suggested that the temperature dependence of Net Primary Production (NPP) is the most important factor in determining land–atmosphere carbon flux. However, precipitation has been suggested, alternatively, as the dominant factor for variation of terrestrial carbon cycle (Tian et al., 1998; Zeng et al., 2005a). On the other hand, studies by Nemani et al. (2003) and Ichii et al. (2005) have indicated that in tropical terrestrial ecosystems, variations in solar radiation and, to a lesser extent, temperature and precipitation, explained most interannual variation in the Gross Primary Production (GPP). Besides these direct biological responses, fire burning due to climate change may play an important role on the variation of total land–atmosphere carbon flux (Langenfelds et al., 2002; Page et al., 2002; Van der Werf et al., 2004). Van der Werf et al. (2004) estimated that during the 1997–1998 El Niño, the anomalous emissions due to fire was 2.1 ± 0.8 PgC of carbon or $66 \pm 24\%$ of the atmospheric CO_2 growth rate anomaly in that period.

Zeng et al. (2005a) have studied the interannual variability of the terrestrial carbon and have suggested that the tropical dominance is a result of a 'conspiracy' between climate and plant/soil physiology. Precipitation and temperature variations in the tropics drive the opposite changes in vegetation growth and soil decomposition, both contributing to land–atmosphere flux changes in the same direction. Though the results of these studies emphasizing the dominant factors influencing the interannual variability of the terrestrial carbon flux vary a lot, they provide insight and opportunities to explore the underlying physical and biological mechanisms of the interannual variability of atmospheric CO_2 growth rate. Most of the studies cited above, however, have primarily focused on the effect of the climatic factors on photosynthetic processes (GPP, NPP). To date, few studies have been conducted on understanding the physical processes in which soil moisture affects the interannual variability of the terrestrial carbon flux. For instance, temperature has a direct impact on vegetation photosynthesis and soil decomposition. On the other hand, the temperature regulates the evapotranspiration and thus influences the variation of soil moisture, which is an important factor for vegetation growth and soil decomposition. Through this, the temperature thus has an indirect impact on the vegetation growth and soil decomposition. This indirect influence has not yet been studied.

The primary purpose of this study is to provide insight into the mechanism of how ENSO-related precipitation and temperature variations regulate vegetation growth, soil respiration and land–atmosphere carbon flux. The following specific scientific questions will be addressed, based on a physical process-based dynamic vegetation and terrestrial carbon model and relevant data sets:

(1) What are the robust spatial and temporal features of the terrestrial carbon cycle in response to ENSO in observations, and can it be simulated by the process-based model? Can this explain the lag in the atmospheric CO_2 growth rate to ENSO?

(2) How do the variations of physical climate (e.g. temperature, precipitation, etc.) associated with ENSO govern terrestrial biophysical processes, such as the vegetation activities and soil decomposition? What are their relative contributions? Can the direct and indirect effect of temperature on the terrestrial carbon flux be quantified?

The paper is organized as follows: Section 2 describes the terrestrial carbon model vegetation-global-atmosphere-soil (VEGAS) and the observational data sets used in this study. In Section 3, we first examine the interannual variability of the

land–atmosphere carbon fluxes by VEGAS, with (1) comparison of the results from inversion models and satellite data; (2) then we apply a composite method and correlation studies to highlight the lead–lag relationship of vegetation response to climatic features on ENSO timescales and (3) finally, we present an investigation of the climatic features that influence the terrestrial carbon cycle with sensitivity studies that delineate the roles of the individual climatic features. Conclusions of the study are presented in Section 4.

2. Models and data

Simulations with the dynamic vegetation and terrestrial carbon model VEGAS coupled to a simple land surface model (SLand), were carried out to investigate the interannual variability of terrestrial response to observational climate variation.

VEGAS simulates the vegetation growth and competition among four different plant functional types (PFTS), namely, broadleaf tree, needle leaf tree, cold grass and warm grass (Zeng, 2003; Zeng et al., 2004; Zeng et al., 2005a,b). The different photosynthetic pathways are distinguished for C3 (the first three PFTs above) and C4 (warm grass) plants. Phenology (or the life cycle of plants) is simulated dynamically as the balance between growth and respiration/turnover. Competition between growths for different PFTs is determined by climatic constraints and resource allocation strategy, such as temperature tolerance and height. The relative competitive advantage then determines fractional coverage of each PFT with possibility of coexistence. Accompanying the vegetation dynamics is the full terrestrial carbon cycle, starting from photosynthetic carbon assimilation in the leaves and the allocation of this carbon into three vegetation carbon pools (or equivalently fuel loads): leaf, root and wood. After accounting for respiration, the biomass turnover from these three vegetation carbon pools cascades into a fast, an intermediate and, finally, a slow soil carbon pool. Temperature- and moisture-dependent decomposition, as well as occurrence of fires, of these fuel loads returns carbon into the atmosphere; thus, closing the terrestrial carbon cycle. In VEGAS, the carbon flux associated with fire burning of vegetation part is included in the respiration of vegetation, and the rest is included in soil decomposition. The key carbon flux outputs from the VEGAS are related as follows:

$$\mathrm{NPP} = \mathrm{GPP} - \mathrm{R_a} \tag{1}$$

$$\mathrm{NEP} = \mathrm{NPP} - \mathrm{R_h} \tag{2}$$

$$\mathrm{F_{ta}} = -\mathrm{NEP} \tag{3}$$

Here GPP is the total amount of carbon fixed by the photosynthesis of the terrestrial ecosystem from the atmosphere. NPP is the carbon fixed after subtracting the respiration of vegetation, called Autotrophic Respiration (R_a), from GPP. The difference of Heteotrophic Respiration (R_h), which is the carbon released due to decomposition of soil organic matter from NPP, is the net ecosystem production (NEP) of the terrestrial ecosystem. F_{ta} is the land–atmosphere carbon flux, otherwise referred to as the net ecosystem exchange (NEE).

SLand (Zeng et al., 1999) is an intermediate-complexity model that consists of two soil layers of temperature and one layer of soil moisture. It includes subgrid-scale parameterizations of the major processes of evapotranspiration, interception loss and surface and subsurface run-off. The validation of modelled soil moisture by SLand on seasonal, interannual and longer timescales can be found in Zeng et al. (2008). In their paper, basin-scale terrestrial water storage for the Amazon and Mississippi basins, diagnosed using the precipitation-evaporation-and-runoff (PER) method from SLand, was compared with those from other land surface models, the reanalysis and National Aeronautics and Space Administration's (NASA's) gravity recovery and climate experiment (GRACE) satellite gravity data. The results indicate that SLand is reliable on seasonal and interannual timescales. In this study, soil wetness (Swet) is used to indicate the water saturation of soil and is defined as a ratio of modelled soil moisture (mm) to the maximum value of 500 mm. Swet varies from 0 to 1.

The physical climate forcing input to the VEGAS includes surface temperature, precipitation, atmospheric humidity, radiation forcing and surface wind. The driving data of precipitation for VEGAS come from a combination of the Climate Research Unit (CRU: New et al., 1999; Mitchell and Jones, 2005) data set for the period of 1901–1979 and the Xie and Arkin (1996) data set of 1980–2006 (which has been adjusted with the 1981–2000 climatology of CRU data set). The surface air temperature driving data use the dataset from the NASA Goddard Institute for Space Studies (GISS) by Hansen et al. (1999), adjusted by CRU climatology of 1961–1990. For the analysis, we focus on the period 1980–2004 in view of the availability of observational normalized difference vegetation index (NDVI) data set and the inversion model results. Seasonal climatology of radiation, humidity and wind speed were used to eliminate the potential CO_2 variability related to these climate fields. Humidity and wind speed are important terms in land surface energy budget; however, its variations have second-order effects on vegetation growth and soil decomposition. There is a large discrepancy of the role of light in terrestrial carbon flux; in particular, even the sign is uncertain. For instance, reduced direct solar radiation during wet periods would reduce photosynthesis (Knorr, 2000) while increased diffuse light under cloudy conditions (e.g. Gu et al., 2003) increases photosynthesis leading to a carbon draw down. We thus chose to include the climatology of light, humidity and wind speed and focus on the effect of the interannual variability of precipitation and temperature in this study. The atmospheric CO_2 concentration for the vegetation photosynthesis was kept constant at pre-industrial level of 280 ppmv since the year-to-year variation of CO_2 level has a small impact on photosynthesis. The advantage of this offline simulation is that

it gives prominence to the terrestrial responses to observed climate better than a fully coupled ecosystem model with model biases of climate, which would in turn affect the carbon module. The resolution of VEGAS is $1.0^\circ \times 1.0^\circ$. The steady-state of model was reached by repeatedly using 1901 climate forcing. At this state, the global total GPP is 124 $PgCyr^{-1}$ with NPP of 61 $PgCyr^{-1}$, and vegetation and soil carbon pools are 641 and 1848 PgC, respectively. These are within the range of observationally based estimates (Schlesinger, 1991). Then this state is used as the initial condition for the 1901–2006 run.

Multivariate ENSO index (MEI) from National Oceanic and Atmospheric Administration (NOAA) is used as an indicator of ENSO signal. MEI is produced, based on six observed variables over the tropical Pacific: sea level pressure; zonal and meridional components of the surface wind; SST; surface air temperature and total cloudiness fraction of the sky (Wolter and Timlin, 1998; Markgraf and Diaz, 2000; http://www.cdc.noaa.gov/ENSO). The uninterrupted CO_2 record for 1965–2006 at Mauna Loa station is used to calculate atmospheric CO_2 growth rate.

The data used to evaluate VEGAS comes from the inversion modelling of Rödenbeck et al. (2003) and the satellite NDVI data. Rödenbeck et al. (2003) estimated CO_2 fluxes by using a time-dependent Bayesian inversion technique, based on 11, 16, 19, 26 and 35 observation sites of atmospheric CO_2 concentration data from NOAA Climate Monitoring and Diagnostics Laboratory and a global atmospheric tracer transport model. A high resolution $1.0^\circ \times 1.0^\circ$ NDVI data set of 1981–2004 from the global inventory modelling and mapping studies (GIMMS) serves to provide a 24-yr satellite record of monthly changes in terrestrial vegetation (Tucker et al., 2001; Zhou et al., 2001; http://gimms.gsfc.nasa.gov/). NDVI is the difference between the advanced very high resolution radiometer (AVHRR) near-infrared and visible bands divided by the sum of these two bands and can be used to quantify the density of plant growth on the Earth. A caveat of the evaluation process is that the evaluating data themselves have limitations. For instance, inversion estimates, themselves, are based on transport models constrained by observational data. Gurney et al. (2003) have found significant differences in carbon flux between different inversion models. Similarly, in the tropics, the satellite produced NDVI data may be deemed suspect because of cloud contamination and saturation of NDVI (Knyazikhin et al., 1998; Myneni et al., 2002). On the other hand, Saleska et al. (2007) have suggested that many terrestrial vegetation and carbon models do not have roots that are deep enough to simulate growth during short-term droughts in the tropics, noticed in observations.

3. Results and discussion

3.1. Interannual variability of terrestrial carbon flux

Interannual fluctuations in SST in the tropical Eastern and Central Pacific are linked to global climate anomalies. For example, the changes of SSTs in the eastern tropical Pacific Ocean and associated deep convection perturb the Hadley circulation and produce a wave train, starting with anomalous upper troposphere divergence in the tropics (Trenberth et al., 1998). Ropelewski and Halpert (1987) examined the link between ENSO events and regional precipitation patterns around the globe and noted that northeastern South America, from Brazil up to Venezuela, had 16 dry episodes during the past 17 ENSO events. Others areas in the tropics, such as Indonesia, Australia, India, etc. also showed a strong tendency to be dry during ENSO events. These dry conditions are usually followed by forest fires and decline of crop yield. Thus, the climate variations associated with ENSO cycle tend to have a strong impact on the terrestrial biosphere in the lower latitudes, especially in the tropical forest areas.

The global and regional F_{ta} simulated by VEGAS (The interannual variability of the time-series of VEGAS and the inversion model is calculated by removing the seasonal cycle and then filtering the data using a 12-month running mean to remove short term fluctuations.) was compared with the corresponding fluxes from the inversion model by Rödenbeck et al. (2003, inversion simulations with 11, 16, 19, 26 and 35 sites. We use the simulation of 11 sites for following ENSO composite analysis because of its longest temporal coverage.) (Fig. 2). Overall, the interannual variability of F_{ta} by VEGAS and the inversion show a good agreement globally, with a correlation of 0.68 (11 sites). A major discrepancy between the VEGAS and inversion is the period after the 1991 Mount Pinatubo eruption (Fig. 2a). The relatively low atmospheric CO_2 growth rate after Mount Pinatubo eruption has been discussed in the past, but a consensus of the underlying mechanism has not yet been reached (Jones and Cox, 2001; Lucht et al., 2002; Gu et al., 2003; Angert et al., 2005). The climatic suppression of respiration by the observed cooling after the eruption, and the enhancement of productivity by changes in diffuse light due to aerosols have been suggested as possible reasons for this discrepancy. Most of the contribution to the global flux comes from the tropics (Fig. 2b). The consistency of VEGAS and the inversion model in the tropics is reflected in the correlation value of 0.55 (11 sites). In contrast to the tropics, the interannual variation in the extratropics is smaller. The terrestrial carbon flux from the Northern Hemisphere extratropics by VEGAS lies within the range of the inversion results (Fig. 2c).

An independent evaluation of the interannual variability of VEGAS was performed by comparing its simulated leaf area index (LAI) to observational NDVI. Many studies have used NDVI data set as an indicator of vegetation growth to address its interannual-to-decadal variability in Northern Hemisphere (Myneni et al., 1998; Tucker et al., 2001; Zhou et al., 2001). LAI is defined as the total leaf area per unit ground area. It is an important canopy parameter for ecosystem studies (Nemani and Running, 1989). In general, there is a close relationship between NDVI and LAI (Wardley and Curran, 1984). The spatial pattern of the temporal correlation of the filtered LAI simulated by VEGAS and the NDVI is indicated in Fig. 3, for the period

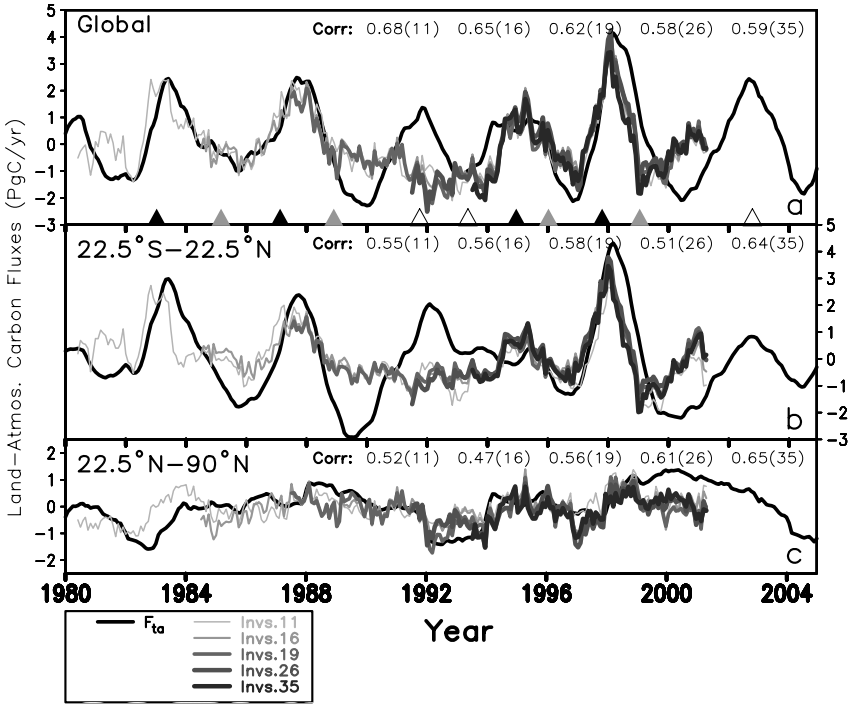

Fig. 2. Interannual variability of land–atmosphere carbon fluxes (F_{ta}) by VEGAS and inversion from Rödenbeck et al. (2003) (lines for the inversion modelling with the CO_2 measurements from 11, 16, 19, 26 and 35 sites) for various regions: (a) Global; (b) Tropics between 22.5°S and 22.5°N and (c) Northern Hemispheric extratropics between 22.5°N and 90°N. Seasonal climatology is calculated based on the 1981–1999 time period for VEGAS and the inversion model, with 11 observational sites; the climatology of the other inversion simulations are calculated with their respective time coverage. The filled triangles represent the ENSO events that have been selected in the composite analysis that follows in the text, with dark triangles for El Niño events and gray for La Niña events. The individual correlation of the land–atmosphere carbon fluxes between VEGAS and the inversion simulation with different number of stations is indicated in the three panels. The value in parenthesis refers to the number stations used in the inversion modelling calculations. All these values are statistically significant at the 90% level of Student's *t*-test.

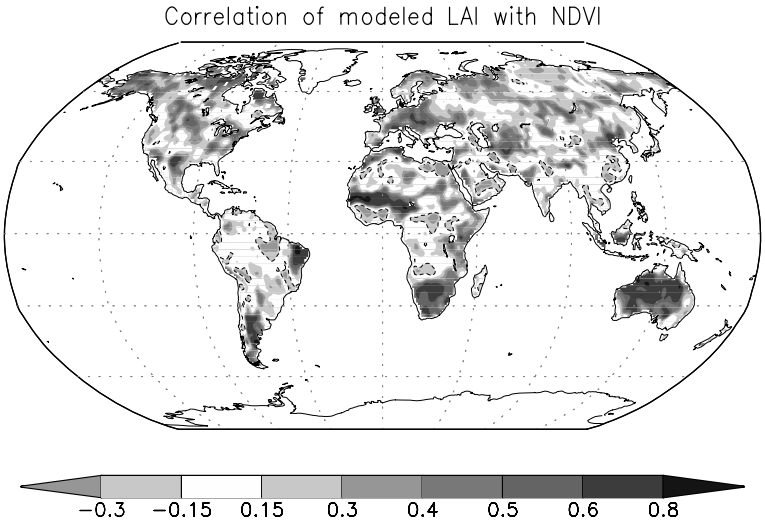

Fig. 3. Evaluation of VEGAS: the spatial pattern of correlation of the VEGAS simulated LAI and the satellite observed NDVI between 1981 and 2004. A contour is used for shaded areas with value smaller than –0.15. Value of 0.33 is statistically significant at the 90% level of Student's *t*-test.

1981–2004. The results indicate that the correlation is higher in Northern and Southern Hemisphere extratropics, whereas it is poorly correlated in the tropics. As cautioned in the previous section, both the observations and model could have problems, which could lead to the poor correlation in the tropics.

3.2. Robust features of the terrestrial response to ENSO

Composite analysis is a useful method in climate studies to highlight the canonical features of a given type of variability, without focusing on the differences between individual events

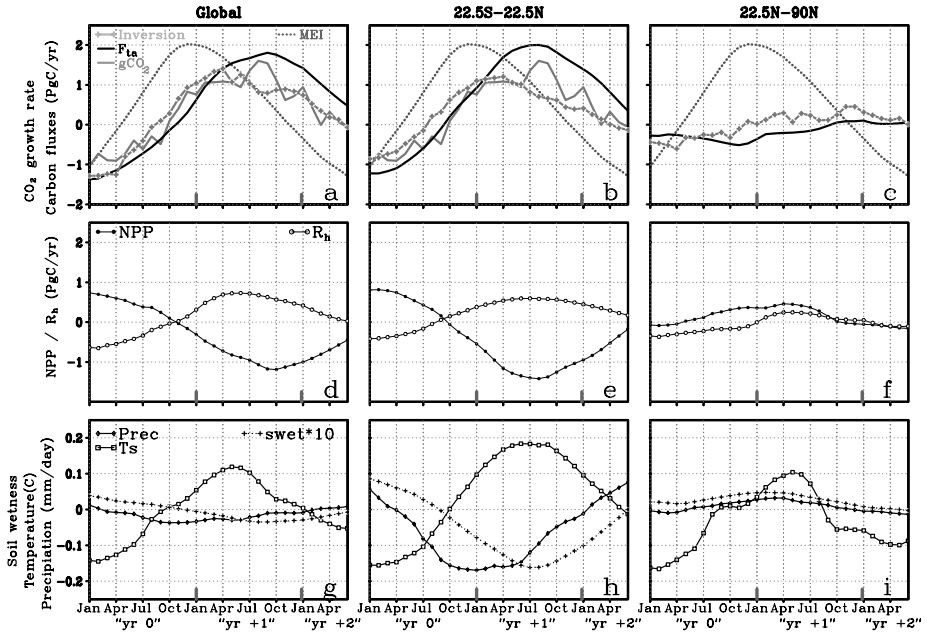

Fig. 4. Composites of the carbon fluxes and the climatic field anomalies during the growth, mature and decaying phases of ENSO. The left-hand (a, d, g), central (b, e, h) and right-hand (c, f, i) panels are the global, the tropical (22.5°S to 22.5°N) and Northern Hemispheric extratropics (22.5°N to 90°N) composites of the terrestrial fields, respectively. The top panels (a, b, c) are the terrestrial land–atmosphere carbon flux anomalies of VEGAS (F_{ta}) and inversion model, the atmospheric CO_2 growth rate (gCO_2) and the reference MEI. The middle panels (d, e, f) are the corresponding Net Primary Production (NPP) and heterotrophic transpiration (R_h), and the bottom panels (g, h, i) are the observed temperature, precipitation and modelled soil wetness (Swet). Unit for carbon fluxes and CO_2 growth rate are $PgCyr^{-1}$, unit for precipitation is mmd^{-1} and temperature is °C, and MEI and soil wetness are non-dimensional. The notation of 'yr 0', 'yr +1', 'yr +2' is the same as in Rassmusson and Carpenter (1982) in which 'yr 0' is the mature phase of ENSO.

(Rasmusson and Carpenter, 1982). Here, similar events are averaged to emphasize the general aspects related to the growth and decay of the event. We used this method to investigate the robust response of the terrestrial ecosystem and associated climate variables during the ENSO cycle. El Niño and La Niña events used in this analysis have values that exceed a *SD* of 0.75, based on the MEI. These events are consistent with the analysis of Trenberth (1997). El Niño occurred in 1982–1983, 1986–1987, 1991–1992, 1993, 1994–1995 and 1997–1998 and La Niña occurred in 1984–1985, 1988–1989, 1995–1996, and 1998–1999. Because of the 1991 Pinatubo eruption, 1991–1992 and 1993 were not included in the following composite analysis. Examination of individual ENSO events indicated that the inter-El-Niño difference can be larger than the difference between typical El Niño and La Niña events. Thus, La Niña events were essentially treated as negative El Niño events and combined to investigate the terrestrial response of ENSO. The composite analysis is similar to that of Rasmusson and Carpenter (1982). To highlight features related to the interannual variability, the composites used in this study were made after the seasonal cycle was removed, and a filter was used to smooth the data. Figure 4 shows a composite of the 2.5-yr time evolution of ENSO events of the observational climate fields and simulated terrestrial responses for the whole globe (left-hand panel), the tropics (central panel) and the Northern Hemisphere extratropics (the right-hand panel). The global total land–atmosphere carbon fluxes from VEGAS (F_{ta}), the inversion model and the atmospheric CO_2 growth rate resemble one another closely during the initiation phase of ENSO and exhibit a 6 month lag with the MEI index (Fig. 4a). The maturity of El Niño occurs in November of 'year 0' of the ENSO event and the peak of inversion flux anomaly lags by 4–5 months, followed by F_{ta} and CO_2 growth rate by 1–2 months later. The tropical land–atmosphere carbon flux anomalies have a similar magnitude and phase as the global fluxes not only in VEGAS simulation but also in inversion model (Fig. 4b). In the tropics, the composite phase of the precipitation anomaly has nearly the same phase as MEI, but the response of modelled soil moisture is delayed because of its memory (Fig. 4h). The simulated vegetation activity (NPP) peaks 6 months after the MEI (Fig. 4e), closer to the phase of soil wetness than to precipitation. On the other hand, modelled soil decomposition R_h also peaks at about a 6 month lag with MEI. As a result, in the model, the decrease of NPP anomaly and increase of R_h anomaly contributes in the same direction and dramatically increase the F_{ta} anomaly during the ENSO warm events. In the mid- and high-latitudes of Northern Hemisphere, VEGAS F_{ta} anomaly phase is in general agreement with inversion flux model results. The response to ENSO is much weaker (Fig. 4c). The variation of precipitation

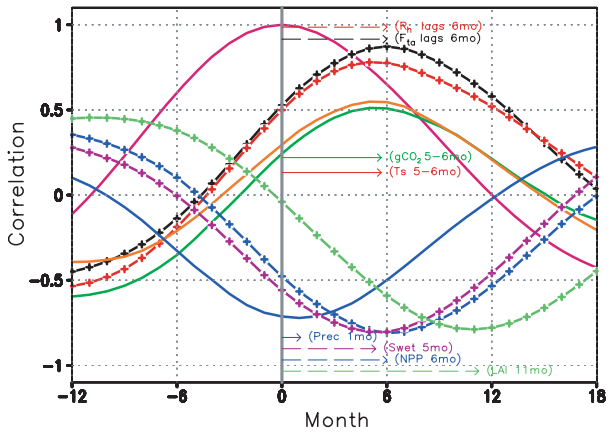

Fig. 5. Lead–lag correlations of tropical terrestrial carbon fluxes and climatic fields with MEI. The observed CO_2 growth rate (gCO_2), temperature, precipitation, modelled NPP, R_h, LAI, F_{ta} and soil wetness are indicated; the solid magenta line is the autocorrelation of MEI with itself. Negative values in *x*-axis represent the number of months the corresponding variables lead the MEI and the positive values denote the number of months the variables lag. Arrows indicate the peak response of each variable. Value of 0.33 is statistically significant at the 90% level of Student's *t*-test.

and temperature are in phase, which is different from the out-of-phase relationship between precipitation and temperature in the tropics.

To better understand the response of the terrestrial ecosystem to ENSO, lead–lag correlations of tropical temperature, precipitation, simulated soil wetness and CO_2 growth rate, as well as terrestrial carbon fluxes with MEI during 1980–2004 were conducted (Fig. 5). In this analysis, only the seasonal cycle was removed from data and no smoothing of the data was performed. This highlights the findings in the central panels of Fig. 4 and gives the exact phase relationship. The peak of the atmospheric CO_2 growth lags MEI about 5–6 months (R = 0.45), similar to Zeng et al. (2005a). In the tropics, observed precipitation closely follows the MEI peak with about 1 month lag (R = –0.83), whereas temperature needs 5–6 months (R = 0.43). Because of the soil memory of water recharge, modelled soil wetness has a 5 month lag. Modelled NPP lags MEI by about 6 months (R = –0.8), with a 11 month lag for LAI by VEGAS, which suggests that vegetation does not show an immediate response to precipitation rather responds to soil wetness closely. On the other hand, R_h follows observed temperature closely and peaks with about a 6 month lag with the MEI. Thus, NPP and R_h simultaneously contribute to the F_{ta} lag of 6 months, with the MEI (R = 0.83) in the tropics in VEGAS. The 'perfect' out of phase relationship of NPP and R_h in the tropics is determined by the anticorrelation of precipitation and temperature pattern associated with ENSO events.

Spatial patterns of the response of VEGAS, 6 months after the peak of the ENSO phase, are shown in Figs. 6a, c, e and g. The tropical regions have robust positive anomalies of land–atmosphere carbon fluxes. The largest positive signals are located in eastern Brazil and equatorial and southern Africa, consistent with the results of Jones et al. (2001). Southeast Asia and the east coast of Australia have sparse positive signals. Overall, the inversion model results (Fig. 6b) and those of VEGAS agree well in the tropics, though there are discrepancies in the extratropics. Modelled LAI from VEGAS and NDVI still show global agreement except in the tropics (Figs. 6c and d). The regions associated with large positive anomalies of F_{ta} regions consistently have large negative NPP anomalies in VEGAS (Fig. 6e) and large positive R_h anomalies (Fig. 6g) in the tropics, such as in the Amazon basin, consistent with the area averaged values in Fig. 4b. These are also regions with correspondingly warm and dry conditions with negative signals of soil wetness (Figs. 6g, h and 4h). Zeng et al. (1999) proposed dynamic and hydrological mechanisms for anticorrelation between precipitation and temperature anomalies in the tropics. Decrease (increase) in precipitation tends to make the land surface dryer (wetter), with less (more) evapotranspiration, less (more) evaporative cooling and then causing higher (lower) temperatures. Increase of absorption of solar radiation due to the absence of cloud during warm ENSO event is also likely to be a candidate for land surface warming.

In the Northern Hemisphere extratropics, temperature anomaly is positively correlated with precipitation anomaly. The response of vegetation to ENSO in the extratropics is small (as seen in Figs. 2 and 4) and does not correspond to the 6-month peak response of vegetation in the tropics. However, interesting features emerge in Fig. 6. North America exhibits a zonal dipole mode of F_{ta} anomalies. In the southwest US, the negative F_{ta} anomaly results from NPP positive anomalies surpassing R_h positive anomalies in strength. In contrast, the F_{ta} anomaly in the northeast US is dominated by negative NPP anomaly and positive R_h anomaly. In the Eurasian continent, weak positive signals exist in East Asia, northwest China, South Europe and northeast Russia. In western Asia, the large negative F_{ta} anomaly is attributable to soil moisture that stimulates the vegetation activities and leads to large positive NPP anomaly. The scenario of other regions is more complex. Other modes of variability, such as the Arctic Oscillation (Buermann et al., 2003), influencing the high latitudes might be a plausible reason for this complex behaviour. It is interesting to note that the spatial pattern of NDVI anomalies generally match LAI anomaly in the middle and high latitudes except northeast of North America, which implies the capability of VEGAS to reproduce the variability of vegetation activities.

The carbon flux associated fire burning is an important fraction of the total terrestrial carbon flux (Langenfelds et al., 2002; Page et al., 2002; Van der Werf et al., 2004). In VEGAS, this carbon flux associated with fire burnt of vegetation part and top soil is included in the respiration of vegetation (R_a) and in soil decomposition (R_h). When fire occurs in VEGAS, leaves burn completely, whereas only part of the wood gets burnt and the

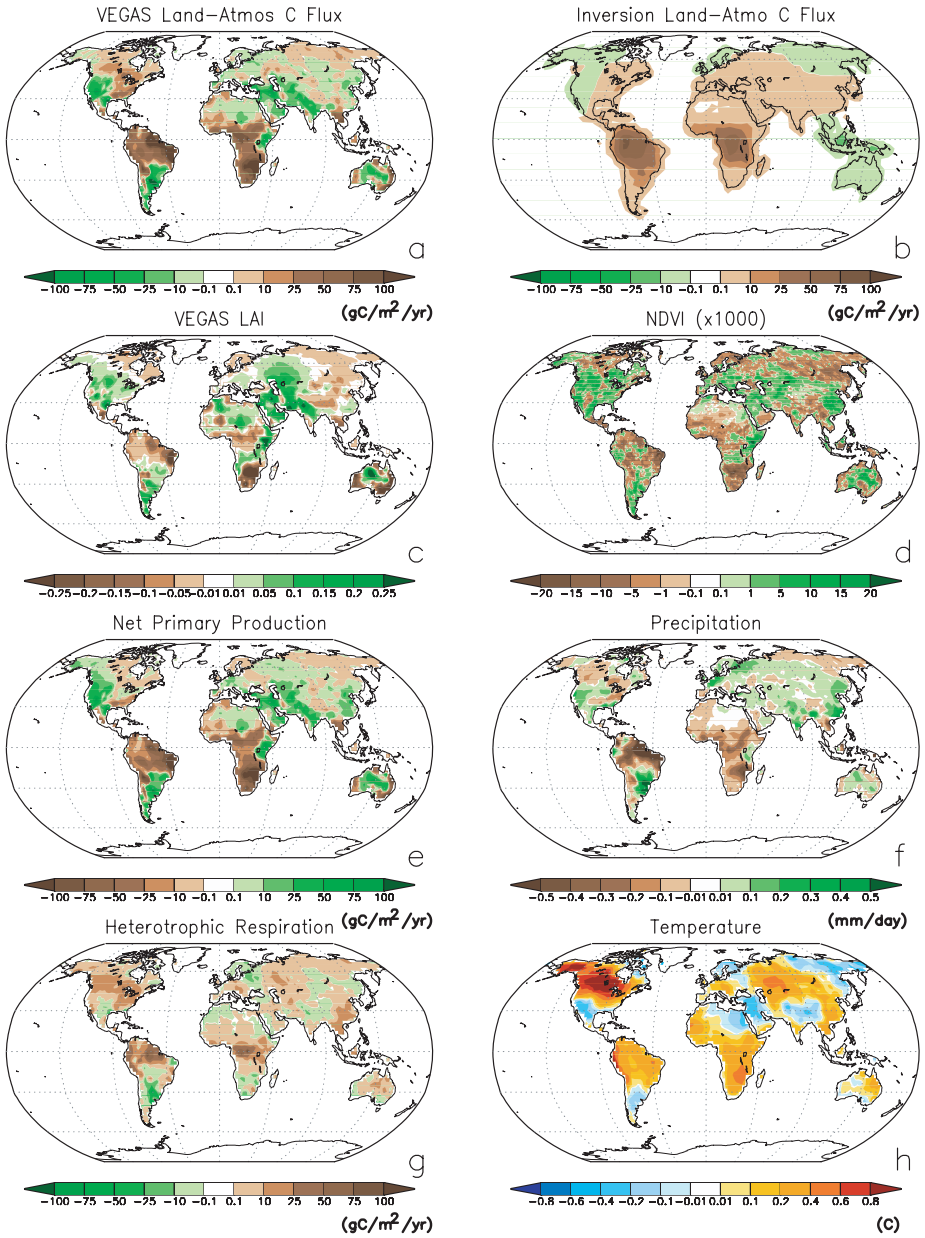

Fig. 6. Spatial patterns of the anomalies of composite variables with 12-month averaging centered at the 6th month after MEI peak (as in Fig. 4a) for: (a) land–atmosphere carbon flux by VEGAS (F_{ta}) in $gCm^{-2}yr^{-1}$; (b) land–atmosphere carbon flux by the inversion in $gC\ m^{-2}yr^{-1}$; (c) LAI by VEGAS; (d) satellite observed NDVI; (e) net primary production (NPP) in $gCm^{-2}yr^{-1}$; (f) Precipitation in mmd^{-1}; (g) Heterotrophic Respiration (R_h) in $gCm^{-2}yr^{-1}$ and (h) Surface air temperature in °C. The shading for NPP is opposite to R_h and F_{ta}.

rest is lumped into the soil carbon pool and fire burns part of top soil. Our simulation shows that the fire burning accounts for about 25% of the total flux anomalies in the tropics during ENSO events (Fig. 7), consistent with Zeng et al. (2005a). About 83% of the fire burnt is included in the R_a and the remaining 17% is included in R_h.

The composite analysis used above has treated La Niña events as the linearly 'opposite' phase of El Niño events, to capture the common features in the response of vegetation to the ENSO cycle. To highlight the differences in the responses between the two phases of the ENSO, composites of El Niño and La Niña events separately are plotted in Fig. 8, for the atmospheric growth rate of CO_2, the land–atmosphere carbon fluxes of VEGAS and inversion model. First of all, for the land–atmosphere carbon fluxes of VEGAS and inversion, CO_2 growth rate agree in phase both in El Niño and La Niña event (Figs. 8a and b). However, the phase evolutions during El Niño and La Niña differ. After La Niña matures, MEI decreases slowly and takes more than

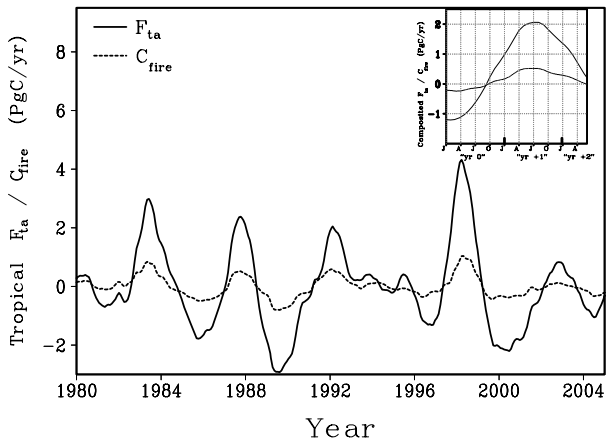

Fig. 7. Time-series of the anomalies of modelled carbon flux due to fire burning and total carbon flux in the tropics. The top right-hand panel is the ENSO composites of these two variables, indicating the contribution of fire burning to total carbon flux anomalies.

1.5 yr to decay. Though the initial increasing time of F_{ta} anomaly in La Niña cycle is only 2 months later than that in El Niño cycle, its maturity takes about half a year more. By examining the evolution of each individual El Niño event since 1980s, we find that El Niño events normally decay quickly in the second year whereas La Niña normally takes longer time to decay. For example, 1982 and 1997 events decayed quickly in July/August of the second year. This quick decay of El Niño normally accompanies a quick change of climate which determines the terrestrial response. Similarly, during La Niña period, the longer persistence of F_{ta}, inversion flux and CO_2 growth rate anomaly is the result of the slower decay of La Niña cycle. Not surprising that the later maturity of global F_{ta} anomaly in ENSO composite comes from La Niña composite contribution. And this situation also can be found in inversion flux and CO_2 growth rate anomalies. Although there are some phase differences of variables during El Niño and La Niña composite, ENSO composite highlights the most important features of terrestrial responses to ENSO cycle.

3.3. Sensitivity simulations to quantify the impact of climatic factors

Physical climatic factors like precipitation, temperature, soil moisture, etc. govern terrestrial carbon cycle. To elucidate and quantify the effects of individual climate forcing, we carefully designed three sensitivity simulations and compared them with the standard simulation (Table 1). The standard simulation is the one in which temperature and precipitation is given from observations, and the results of these were discussed in the previous section. A 'climatology' simulation in which the precipitation and temperature climatology is fixed, provides input to one of the three sensitivity simulations. The sensitivity simulations are as follows: (1) 'P-only experiment' uses the observed precipitation while using the climatology of temperature; (2) 'T-only experiment' uses the observed temperature while using precipitation climatology and (3) 'Swet-fixed experiment' in which, in addition to 'T-only experiment', soil moisture is provided with the climatology from the 'climatology' simulation, rather than the one simulated by the land–surface module in 'T-only experiment'. This climatology comes from the 'climatology' simulation described earlier. So, vegetation photosynthesis will see the

Table 1. Changes in physical climate forcing (temperature/precipitation) in the sensitivity simulations

Experiment	Physical climate forcing
Climatology	Climatology of temperature and precipitation, and soil moisture is simulated by SLand.
Standard	Observed temperature and precipitation, and soil moisture is simulated by SLand.
P-only	Observed precipitation while using the climatology of temperature, and soil moisture is simulated by SLand.
T-only	Observed temperature while using precipitation climatology and soil moisture is simulated by SLand.
Swet-fixed	In addition to 'T-only', soil moisture is provided with the climatology from the 'climatology' experiment rather than modelled by SLand as in 'T-only'.

Note: The same seasonal climatology of radiation, humidity and wind speed, as well as constant CO_2 level for VEGAS, were used in all following experiments

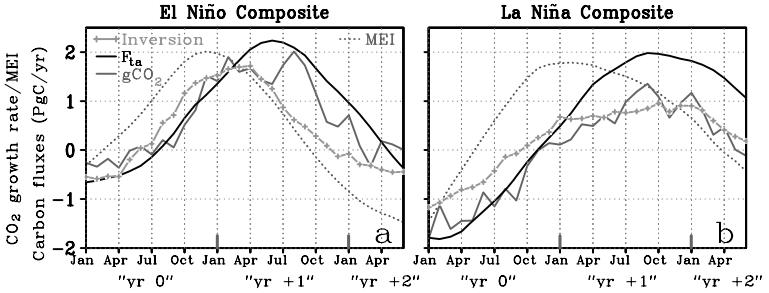

Fig. 8. Tropical composites for (a) El Niño events only: 1982–1983, 1986–1987, 1994–1995, 1997–1998 and (b) La Niña event only: 1984–1985, 1988–1989, 1995–1996, 1998–1999. The selected variables are the same as Fig. 4b.

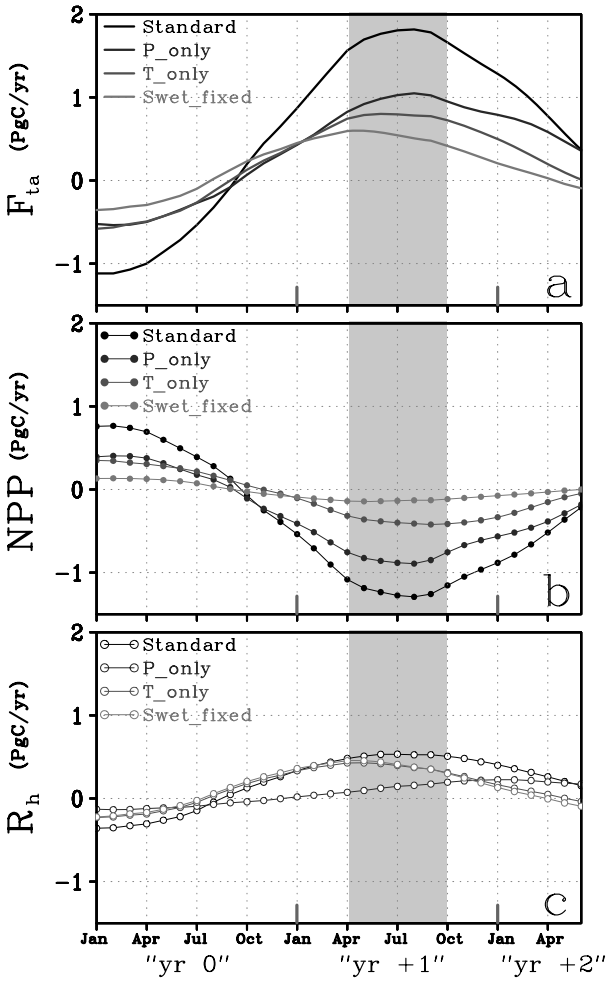

Fig. 9. ENSO-composites of carbon fluxes for the sensitivity simulations: (a) the VEGAS F_{ta} response in the tropics for the standard, 'P-only', 'T-only' and 'Swet-fixed' sensitivity simulations; (b) the same as (a) except for NPP and (c) the same as (a) except for heterotrophic respiration. The shaded period of April–September of 'yr +1' is the maximum regime of the response to ENSO cycle. The carbon fluxes averaged in this regime are indicated in Table 2, in $PgCyr^{-1}$.

variation of temperature; whereas the soil moisture changes due to evapotranspiration by temperature is excluded from vegetation photosynthesis. This 'Swet-fixed' simulation thus informs us of the indirect temperature effect on NPP through soil moisture, in contrast to the 'T-only' simulation, which includes both the direct and indirect effect of temperature through soil moisture on NPP.

ENSO composites of these sensitivity simulations help quantify the effects of temperature, precipitation and soil wetness on NPP/ R_h / F_{ta} and are shown in Fig. 9, for the tropics. The period of maximum response (April to September of the 'year +1') of the ENSO event is highlighted, the averaged values of those periods are calculated (Table 2) and the percentage contribution of each climatic factor on F_{ta} is also provided (Fig. 10). The period selected is based on the composite analysis and the lead–lag correlation in Section 3.2.

The mean global total of the F_{ta} anomaly for the selected period in the standard run is 1.68 $PgCyr^{-1}$, which is a little larger than that of the inversion model flux with 1.36 $PgCyr^{-1}$ (Table 2). Both of them are larger than actual CO_2 growth rate, which is 1.22 $PgCyr^{-1}$. This difference can be attributable to the net oceanic carbon uptake from the atmosphere during El Niño event and is within the range of previous estimates (Keeling and Revelle, 1985; Winguth et al., 1994; Bousquet et al., 2000; Feely et al., 2002).

The tropical land–atmosphere carbon flux dominates global total both in VEGAS and in the inversion model. However, in the standard VEGAS simulation, the extratropics acts as a relatively small carbon sink whereas the inversion model indicates it as a small carbon source. In the tropics, out of the 1.77 $PgCyr^{-1}$ F_{ta} variation, 1.21 $PgCyr^{-1}$ comes from the suppression of vegetation (NPP) and the rest 0.56 $PgCyr^{-1}$ from the soil decomposition (Figs. 9b and c). Our sensitivity simulations show a highly linear relationship of the effects of anomalous temperature and precipitation on the terrestrial carbon cycle, particularly at the peak of the response. In reality, such effects, however, are extremely complicated and not well known. One possible reason is that the interannual variability can be considered as a small perturbation to the system (VEGAS), which itself is highly nonlinear. Assuming an approximately linear relationship, we can estimate that precipitation contributes about 1.0 $PgCyr^{-1}$, while temperature provides about 0.79 $PgCyr^{-1}$ of the F_{ta} variation in standard simulation. In the tropics, the 'P-only' sensitivity experiment produced a change of –0.86 $PgCyr^{-1}$ for the NPP anomaly, whereas soil decomposition decreases dramatically to 0.14 $PgCyr^{-1}$ from 0.56 $PgCyr^{-1}$ during this period. In the 'T-only' simulation, the soil decomposition is remarkably enhanced due to warming, although less reduction of vegetation activity is seen. Spatially, the distribution of the regions with remarkable reduction of NPP in 'P-only' is similar to the one in standard run, albeit with a smaller intensity (figures not shown). Compared with standard run, the regions with positive signal of soil decomposition shrink to Northern South America and Central Africa, in 'P-only' run. The remarkable enhancements of soil decomposition due to warming and dramatic vegetation suppression due to drought lies in the nature of the tropics: highly-decomposing and water-limited.

The absorption of water for vegetation depends on the water pressure level difference between the soil moisture and vegetation root. Thus, vegetation activity closely follows soil moisture, rather than immediately responding to precipitation. However, soil moisture can be influenced by temperature through evapotranspiration. Thus, precipitation affects NPP mainly through soil wetness, whereas temperature can influence NPP variation through soil moisture. In the 'Swet-fixed' simulation, only –0.13 $PgCyr^{-1}$ of NPP occurs compared with the –0.34 $PgCyr^{-1}$ reduction in the 'T-only' simulation, which reflect the indirect effect of

Table 2. Mean of composite global and tropical carbon fluxes during the peak response to ENSO (shaded area in Fig. 9 corresponding to the 6 month average from April to September of 'yr +1') for VEGAS standard, 'P-only', 'T-only', 'Swet-fixed' experiments and CO_2 growth rate (in $PgCyr^{-1}$)

Region	Rödenbeck[a] RF	Standard F_{ta} (NPP/R_h)	P-only F_{ta} (NPP/R_h)	T-only F_{ta} (NPP/R_h)	Swet-fixed F_{ta} (NPP/R_h)
Global	1.36	1.68(−0.99/0.69)	0.74(−0.65/0.09)	0.95(−0.34/0.60)	0.79(−0.17/0.62)
Tropics	1.19	1.77(−1.21/0.56)	1.00(−0.86/0.14)	0.79(−0.34/0.44)	0.59(−0.13/0.46)
gCO_2	1.22				

[a]Rödenbeck inversion modelling with 11 station measurements.

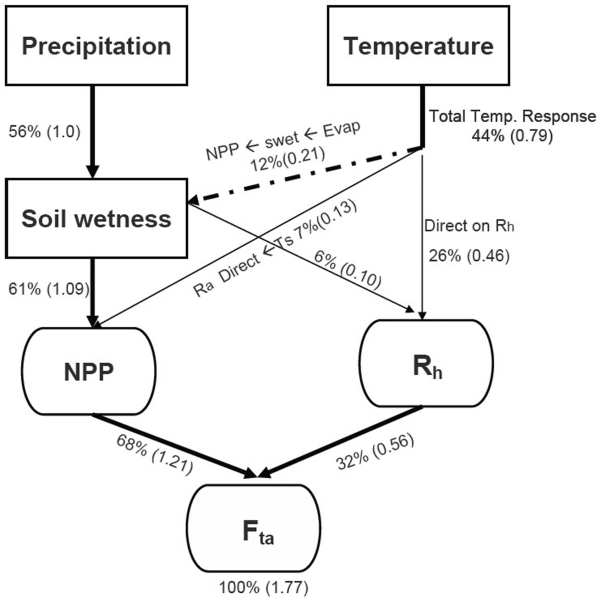

Fig. 10. A conceptual diagram of the mechanism of tropical terrestrial carbon response to the ENSO cycle. The percentages refer to the contribution to F_{ta} variation (100%), with carbon flux anomalies in parenthesis (Unit in $PgCyr^{-1}$). These carbon fluxes are estimated from Table 2. The climate fields, such as precipitation, temperature and soil wetness are shown as rectangles and the corresponding NPP/R_h/F_{ta} as rounded rectangle. The dashed arrow indicates the indirect effect of temperature on NPP through soil wetness. The solid lines in black from temperature are the direct effects of temperature on soil decomposition and on NPP. All processes are contributable to F_{ta} in the same direction (for example, increase of soil decomposition and decrease of vegetation growth during El Niño).

temperature on the NPP through soil moisture. Spatially, the central Amazon basin and South Africa have much less vegetation suppression in the 'Swet-fixed' run (spatial pattern not shown). The 'Swet-fixed' sensitivity experiment indicates clearly that the indirect effect of temperature on the vegetation photosynthesis through soil wetness is significant; even a little larger than the direct temperature affect the photosynthetic processes in the tropics in model. This is interesting because the tropics always have favourable temperature condition for vegetation around the year, whwhereas the change in water supply during the ENSO period can drastically affect the vegetation growth.

Fig. 10 is a schematic diagram of the percentage of relative contribution of the individual and combined effects of precipitation and temperature on the variation of F_{ta} in the tropics during ENSO. Values used to calculate the percentages were obtained from Table 2, which correspond to a 6 month average (April to September) at the peak of the ENSO response. Some are obtained as a direct result of the simulations, whereas the rest are obtained as residuals.

The tropical ENSO response of the total carbon flux into the atmosphere is a result of photosynthesis (68%) and soil decomposition (32%), as obtained from the standard simulation. We estimated that among the total land–atmosphere carbon flux, about 25% is due to fire burning, which is included in the vegetation and soil respiration. Precipitation is the major contributor to photosynthesis whereas temperature is to soil decomposition. In terms of 100% variation of F_{ta}, precipitation contributes about 56% variation, mainly through soil wetness in photosynthesis, whereas temperature accounts for 44% totally as seen from the total flux of the 'P-only' and 'T-only' experiments. The total effect of temperature arises from direct and indirect effects. The direct effect is through a 26% influence on soil respiration and a 7% influence on respiration of vegetation, as obtained from the 'Swet-fixed experiment'. The remaining contribution of temperature is through its indirect effect in which photosynthesis is affected by temperature changes affecting evaporation and thus changing soil moisture. This indirect effect of temperature is 12% and is obtained as the difference between the 'Swet-fixed' and 'T-only' experiment. This indirect effect is highly complicated and has not been studied in the past. The total effect of soil wetness on the total flux into the atmosphere is obtained as a residual of the remaining terms, and 61% affects photosynthesis, while 6% affects soil decomposition.

4. Conclusions

In this study, we use a dynamic vegetation and terrestrial carbon model VEGAS to investigate the response of the terrestrial carbon cycle to the physical climate variations and to isolate those effects, especially the ones associated with ENSO. The results

of the model are first evaluated against observations to verify its capability in capturing the interannual variability. The simulated F_{ta} in our study agrees well with the results of inversion modelling based on the observations on interannual timescale, especially in the tropics. Both of them are in agreement with the atmospheric CO_2 growth rate variation. The simulated LAI by VEGAS has good correlation with observed NDVI in the extratropics. The land–atmosphere carbon flux in the tropics has a similar magnitude as the global total, confirming the dominant role of the tropics on interannual timescale. This underscores the importance of observational network of the tropics in the future.

Our analysis of ENSO composite and lead–lag correlation indicates that in the tropics, VEGAS simulates a robust signal of F_{ta} with a 6 month lag of ENSO cycle. This is largely caused by the suppression of vegetation and enhancement of soil decomposition, as suggested by the 'conspiracy' theory of Zeng et al. (2005a). Though the anomalous precipitation lags ENSO cycle by 1–2 months, the vegetation-dependent soil moisture takes about 5 months to respond, due to soil memory. Less precipitation, with higher temperature, drains the soil moisture and results in drought condition, unfavourable for vegetation activities. This results in a 6-month lag of the NPP to ENSO. During El Niño, large areas of vegetation suppression occur in Brazil, equatorial Africa and South Africa. Simultaneously, higher temperature directly enhances soil decomposition in northern Brazil and equatorial Africa. As a result, reduction of NPP and enhancement of R_h contributes in same direction and provide a large amount of carbon release to the atmosphere. The opposite is true for La Niña.

Sensitivity simulations were performed to elucidate and quantify the effects of precipitation and temperature on the tropical terrestrial ecosystem. During ENSO events, the precipitation and temperature has very different mechanisms in regulating the above variation of vegetation growth and soil decomposition. A near linear relationship of terrestrial carbon response to the anomalous precipitation and temperature was found in model. In total, precipitation variation contributes about 56% of F_{ta} variation, mostly through soil wetness in the photosynthesis process, whereas temperature accounts for 44%, which includes 25% from direct effect on the soil decomposition, 7% from direct effect on vegetation respiration and 12% from indirect effect on the photosynthesis through soil wetness. Such an indirect effect is significant but has not been studied in the past. As a result, in the tropics vegetation activity, suppression (NPP) contributes 68% of variation of F_{ta}, with the remaining 32% coming from soil decomposition under a warming and drought condition. Among the total land–atmosphere carbon flux, about 25% is due to fire burning, which is included in the vegetation and soil respiration.

Due to spatial cancellation and weak ENSO teleconnections, the response of terrestrial system in middle and high latitudes are less robust and more complex. The interannual variability of the land–atmosphere carbon flux in the extratropics is complicated by other modes of climate variability, such as the Pacific North American pattern of variability, the Atlantic Oscillation and Northern Annular Mode (Buermann et al., 2003; Potter et al., 2003; Russell and Wallace, 2004). Moreover, the role of solar radiation for vegetation is still in debate and has not been addressed in this study (Gu et al., 2003; Angert et al., 2005).

The results in this study are based on a single vegetation model and hence could be model-dependent. Yet it has been useful in addressing the canonical response of the terrestrial carbon flux to ENSO. The linear response observed in the tropics helped quantify the mechanisms through which precipitation and temperature affect the carbon flux directly and indirectly, thus highlighting the importance of soil moisture on vegetation. Improved observations and advanced modelling studies are required to quantify exactly the terrestrial carbon cycle under changing climate.

5. Acknowledgments

We have benefited from stimulating discussions with J-H. Yoon, A. Mariotti. We are grateful to C. Jones and an anonymous reviewer and the editor, Harald Lejenäs, for their comments and suggestions that have helped improve the presentation and quality of the paper. C. Rödenbeck kindly provided their inversion data for comparison. This research was supported by NSF grant ATM0739677, NOAA grants NA04OAR4310091 and NA04OAR4310114 and NASA grant 407191AG7.

References

Angert, A., Biraud, S., Bonfils, C., Henning, C. C., Buermann, W. and co-authors. 2005. Drier summers cancel out the CO_2 uptake enhancement induced by warmer springs. *Proc. Natl. Acad. Sci. USA* **102**(31), 10823–10827.

Bacastow, B. R. 1976. Modulation of atmospheric carbon dioxide by the Southern Oscillation. *Nature* **261**, 116–118.

Bousquet, P., Peylin, P., Ciais, P., LeQuere, C., Friedlingstein, P. and co-authors. 2000. Regional changes in carbon dioxide fluxes of land and oceans since 1980. *Science* **290**, 1342–1346.

Braswell, B., Schimel, D., Linder, E. and Moore, B. 1997. The response of global terrestrial ecosystems to interannual temperature variability. *Science* **278**, 870–872.

Buermann, W., Anderson, B. and Tucker, C. 2003. Interannual covariability in northern hemisphere air temperatures and greenness associated with El Niño-Southern Oscillation and the Arctic Oscillation. *J. Geophys.* **108**, doi:10.1029/2002JD002630.

Feely, R., Boutin, J., Cosca, C. E., Dandonneau, Y., Etcheto, J. and co-authors. 2002. Seasonal and interannual variability of CO_2 in the equatorial Pacific. *Deep Sea Res. Part II Top. Stud. Oceanogr.* **49**(13–14), 2443–2469.

Gu, L., Baldocchi, D. D., Wofsy, S., Munger, J. W., Michalsky, J. J., and co-authors. 2003. Response of a deciduous forest to the Mount Pinatubo eruption: enhanced photosynthesis. *Science* **299**, 2035–2038.

Gurney, K. R., Law, R. M., Denning, A. S., Rayner, P. J., Baker, D. and coauthors. 2003. Transcom 3 CO_2 inversion intercomparison: 1.

Annual mean control results and sensitivity to transport and prior flux information. *Tellus* **55B**, 555–579.

Hansen, J., Ruedy, R., Glascoe, J. and Sato, M. 1999. GISS analysis of surface temperature change. *J. Geophys. Res.* **104**, 30997–31022.

Ichii, K., Hashimoto, H., Nemani, R. and White, M. 2005. Modeling the interannual variability and trends in gross and net primary productivity of tropical forests from 1982 to 1999. *Glob. Planet. Change* **48**(4), 274–286.

Jones, C. D. and Cox, P. M. 2001. Modeling the volcanic signal in the atmospheric CO_2 record. *Global Biogeochem. Cycles* **15**(2), 453–465.

Jones, C., Collins, M., Cox, P. and Spall, S. 2001. The carbon cycle response to ENSO: a coupled climate-carbon cycle model study. *J. Clim.* **14**(21), 4113–4129.

Joseph, R. and Nigam, S. 2006. ENSO evolution and teleconnections in IPCC's twentieth-century climate simulations: realistic representation? *J. Clim.* **19**, 4360–4377.

Keeling, D. C. and Revelle, R. 1985. Effects of El Niño/Southern Oscillation on the atmospheric content of carbon dioxide. *Meteoritics* **20**(no.2, pt.2), 437–450.

Kindermann, J., Wurth, G., Kohlmaier, G. and FW, B. 1996. Interannual variation of carbon exchange fluxes in terrestrial ecosystems. *Global Biogeochem. Cycles* **10**(4), 737–755.

Knorr, W. 2000. Annual and interannual CO_2 exchanges of the terrestrial biosphere: process-based simulations and uncertainties. *Global Ecol. Biogeogr.* **9**(3), 225–252.

Knyazikhin, Y., Martonchik, J. V., Diner, D. J., Myneni, R. B., Verstraete, M. and co-authors. 1998. Estimation of vegetation canopy leaf area index and fraction of absorbed photosynthetically activeradiation from atmosphere-corrected MISR data. *J. Geophys. Res.* **103**, 32239–32256.

Langenfelds, R. L., Francey, R. J., Pak, B. C., Steele, L. P., Lloyd, J. and co-authors. 2002. Interannual growth rate variations of atmospheric CO_2 and its $\delta^{13}C$, H_2, CH_4, and CO between 1992 and 1999 linked to biomass burning. *Global Biogeochem. Cycles* **16**(3), 1048, doi:10.1029/2001GB0011466.

Lucht, W., Prentice, I., Myneni, R., Sitch, S., Friedlingstein, P., and co-authors. 2002. Climatic control of the high-latitude vegetation greening trend and Pinatubo effect. *Science* **296**, 1687–1689.

Markgraf, V. and Diaz, H. F. 2000: The past ENSO record: a synthesis. In: *El Niño and the Southern Oscillation: Multiscale Variability and Global and Regional Impacts* (eds. H. F. Diaz and V. Markgraf). Cambridge University Press, Cambridge, UK, 465–488.

Mitchell, T. D. and Jones, P. D. 2005. An improved method of constructing a database of monthly climate observations and associated high-resolution grids. *Int. J. Climatol.* **25**, 693–712.

Myneni, R. B., Tucker, C. J., Asrar, G. and Keeling, C. D. 1998. Interannual variations in satellite-sensed vegetation index data from 1981 to 1991. *J. Geophys. Res.-Atmos.* **103**(D6), 6145–6160.

Myneni, R. B., Hoffman, S., Knyazikhin, Y., Privette, J. L., Glassy, J. and co-authors. 2002. Global products of vegetation leaf area and fraction absorbed PAR from year one of MODIS data. *Remote Sens. Environ.* **83** (1–2), 214–231.

Nemani, R. R. and Running, S. W. 1989. Testing a theoretical climate-soil-leaf area hydrologic equilibrium of forests using satellite data and ecosystem simulation. *Agric. For. Meteorol.* **44**, 245–260.

Nemani, R., Keeling, C., Hashimoto, H., Jolly, W., Piper, S., and co-authors. 2003. Climate-driven increases in global terrestrial net primary productivity from 1982 to 1999. *Science* **300**, 1560–1563.

New, M., Hulme, M. and Jones, P. 1999. Representing twentiethcentury space–time climate variability. Part I: development of a 1961–90 mean monthly terrestrial climatology. *J. Clim.* **12**, 829–856.

Page, S. E., Siegert, F., Rieley, J. O., Boehm, H.-D. V., Jaya, A. and co-authors. 2002. The amount of carbon released from peat and forest fires in Indonesia during 1997. *Nature* **420**, 61–65.

Potter, C., Klooster, S., Steinbach, M., Tan, P., Kumar, V. and co-authors. 2003. Global teleconnections of climate to terrestrial carbon flux. *J. Geophys. Res.* **108**, doi:10.1029/2002JD002979.

Rasmusson, E. M. and Carpenter, T. H. 1982. Variations in tropical sea surface temperature and surface wind fields associated with the Southern Oscillation/El. Niño. *Mon. Wea. Rev.* **110**, 354–384.

Rayner, P., Law, R. and Dargaville, R. 1999. The relationship between tropical CO_2 fluxes and the El Niño-Southern Oscillation. *Geophys. Res. Lett.* **26**(4), 493–496.

Ropelewski, C. F. and Halpert, M. S. 1987. Global and regional scale precipitation patterns associated with the El Niño/Southern Oscillation. *Mon. Wea. Rev.* **115**, 1606–1626.

Rödenbeck, C., Houweling, S., Gloor, M. and Heimann, M. 2003. CO_2 flux history 1982-2001 inferred from atmospheric data using a global inversion of atmospheric transport. *Atmos. Chem. Phys.* **3**, 1919–1964.

Russell, J. L. and Wallace J. M. 2004. Annual carbon dioxide drawdown and the Northern Annular Mode. *Global Biogeochem. Cycles* **18**, GB1012, doi:10.1029/2003GB002044.

Saleska, S., Didan, K., Huete, A. and da Rocha, H. 2007. Amazon Forests green-up during 2005 drought. *Science*, doi:10.1126/science.1146663.

Schlesinger, W. 1991. *Biogeochemistry: An Analysis of Global Change*. Academic Press, San Diego.

Tian, H., Melillo, J., Kicklighter, D., McGuire, A., Helfrich, J. and co-authors. 1998. Effect of interannual climate variability on carbon storage in Amazonian ecosystems. *Nature* **396**, 664–667.

Trenberth, K. E. 1997. The definition of El Niño. *Bull. Amer. Met. Soc.* **78**, 2771–2777.

Trenberth, K. E., Branstator, G. W., Karoly, D., Kumar, A., Lau, N. C. and co-authors. 1998. Progress during TOGA in understanding and modeling global teleconnections associated with tropical sea surface temperatures. *J. Geophys. Res.* **103**, 14291–14324.

Tucker, C. J., Slayback, D. A., Pinzon, J. E., Los, S. O., Myneni, R. B. and co-authors. 2001. Higher northern latitude normalized difference vegetation index and growing season trends from 1982 to 1999. *Int. J. Biometeorol.* **45**(4), 184–190.

Van der Werf, G., Randerson, J., Collatz, G., Giglio, L., Kasibhatla, P. and co-authors. 2004. Continental-scale partitioning of fire emissions during the 1997 to 2001 El Niño/La Niña period. *Science* **303**, 73–76.

Wardley, N. W. and Curran, P. J. 1984. The estimation of green leaf area index from remotely sensed airborne multiespectral scanner data. *Int. J. Remote Sens.* **5**(4), 671–679.

Winguth, A., Heimann, M., Kurz, K., Maier-Reimer, E., Mikolajewicz, U. and co-authors. 1994. El Niño-Southern Oscillation related fluctuations of the marine carbon cycle. *Global Biogeochem. Cycles* **8**, 39–64.

Wolter, K. and Timlin, M. S. 1998. Measuring the strength of ENSO events—how does 1997/98 rank? *Weather* **53**, 315–324.

Xie, P. and Arkin, P. A. 1996. Analyses of global monthly precipitation using gauge observations, satellite estimates, and numerical model predictions. *J. Clim.* **9**, 840– 858.

Zeng, N. 2003. Glacial-interglacial atmospheric CO_2 CHANGE—the glacial burial hypothesis. *Adv. Atmos. Sci.* **20**, 677–693.

Zeng, N., Neelin, J. D., Lau, K.-M. and Tucker, C. T. 1999 Enhancement of interdecadal climate variability in the Sahel by vegetation interaction. *Science* **286**, 1537–1540.

Zeng, N., Qian, H., Munoz, E. and Iacono, R. 2004. How strong is carbon cycle-climate feedback under global warming? *Geophys. Res. Lett.* **31** L20203, doi:10.1029/2004GL020904.

Zeng, N., Mariotti, A. and Wetzel, P. 2005a. Terrestrial mechanisms of interannual CO_2 variability. *Global Biogeochem. Cycles* **19**, doi:10.1029/2004GB002273.

Zeng, N., Qian, H., Rödenbeck and Heimann, M. 2005b. Impact of 1998-2002 midlatitude drought and warming on terrestrial ecosystem and the global carbon cycle. *Geophys. Res. Lett.* **32**, doi:10.1029/2005GL024607.

Zeng, N., Yoon, J-H. Mariotti, A. and Swenson, S. 2008. Long-term soil moisture variability from a new P-E water budget method. *J. Clim.* **15**, 248–265.

Zhou, L. M., Tucker, C. J., Kaufmann, R. K., Slayback, D. V., Shabano, N. and co-authors. 2001. Variations in northern vegetation activity inferred from satellite data of vegetation index during 1981 to 1999. *J. Geophys. Res.* **106**(D17), 20069–20083.